EVS28
KINTEX, Korea, May 3-6, 2015

Sensitivity analysis for assessing robustness of position-based predictive energy management strategy for fuel cell hybrid electric vehicle

Jihun Han[1], Dongsuk Kum[2], and Youngjin Park[1]
[1]*Department of Mechanical Engineering, Korea Advanced Institute of Science and Technology (KAIST), 291 Daehak-ro, Yueong-gu, Daejeon 305-701, Republic of Korea, heykeke@kaist.ac.kr*
[2]*The Cho Chun Shik Graduate School of Green Transportation, KAIST, 291 Daehak-ro, Yuseong-gu, Daejeon 305-701, Republic of Korea*

Abstract

Under hilly road conditions, it is difficult to achieve near-optimal performance of energy management strategy (EMS) of fuel cell hybrid electric vehicle (FCHEV). In order to achieve near-optimality, optimal state reference trajectory is predicted based on future information, and thus reference tracking controller is often considered as real-time predictive EMS. There are two approaches depending on in what way the predicted reference will be used as follows: 1) position-based predictive EMS for tracking position-dependent reference, 2) time-based predictive EMS for tracking time-dependent reference. In this paper, analytical sensitivity analysis based on Pontryagin's minimum principle (PMP) is performed to prove robustness of position-based predictive EMS with respect to velocity uncertainty. First, optimal control problem is formulated in time and position domain, and PMP approach is used to derive boundary value problem (BVP) that achieves global optimality. Then, sensitivity differential equations are developed which describe sensitivity of original BVP with respect to velocity uncertainty. Finally, these equations will be solved simultaneously with the original BVP to compute first-order sensitivity of time- and position-dependent optimal state. Results show that sensitivity of time-dependent optimal state is much bigger than that of position-dependent optimal state because velocity uncertainty can change predicted travel time, and this effect on sensitivity is significant. Therefore, predictive EMS should use current position to track position-dependent optimal state reference in terms of the robustness with respect to velocity uncertainty.

Keywords: FCHEV (fuel cell hybrid electric vehicle), PMP (Pontryagin's minimum principle), Position-based predictive energy management strategy, Sensitivity Analysis

1 Introduction

Generally, fuel cell-powered vehicles are equipped with additional energy storage system, which are often called as fuel cell hybrid electric vehicle (FCHEV). Energy management strategy (EMS) of FCHEVs determines power split ratio between the two energy sources for improving FCHEV system efficiency. A number of EMSs has been widely studied for a decade [1], as follows: rule-based approach [2-4], horizon-optimization approach such as dynamic programming (DP) [5-7] and Pontryagin's minimum principle (PMP) [8,9], and instantaneous (real-time) optimization approach such as equivalent consumption minimization strategy (ECMS) [10-12].

Under hilly road conditions, it is difficult to achieve near-optimal performance of real-time EMS using current driving information because upcoming potential energy cannot be predicted [13,14]. As an alternative to achieve near-optimality, globally optimal state reference trajectory is predicted by using future information, and EMS will track this reference. Note that future information is considered as altitude profile and the predicted velocity profile [15,16] using global positioning system (GPS), geographic information systems (GIS), and transportation systems (ITS). For example, in ECMS framework, adaptation law of equivalent factor is designed as state feedback controller for tracking the predicted state reference trajectory [17-19].

If planned route is fixed during driving, altitude profile cannot be changed, but there must be velocity uncertainty between real and the predicted velocity profile under real-world driving conditions. Therefore, robustness toward velocity uncertainty becomes important issue for real-time predictive EMS. There are two approaches depending on in what way the predicted reference will be used as follows: the first one is position-based predictive EMS for tracking position-dependent reference, second one is time-based predictive EMS for tracking time-dependent reference. Figure 1 schematically illustrates the predictive EMS as reference tracking controller.

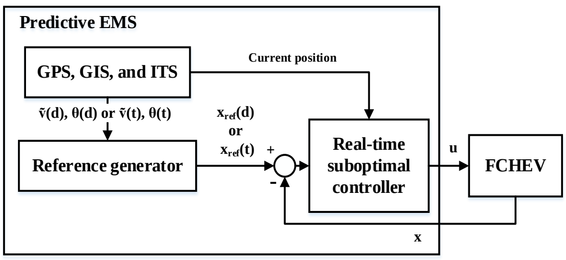

Figure 1: Overview of predictive EMS

There is the belief that robustness of position-based predictive EMS outperforms that of time-based predictive EMS because velocity uncertainty can change travel time, but cannot do travel position. However, analytical approach has not been reported to prove the robustness of position-based predictive EMS in comparison with time-based predictive EMS. Because predictive EMSs must correct state from reference, it will experience large loss of optimality when velocity uncertainty presents. For this reason, optimal state sensitivity with respect to velocity uncertainty is directly linked to the robust performance of predictive EMS. Therefore, in this paper, comparative analysis for sensitivity of time- and position-dependent optimal state is performed to confirm and prove the robustness of position-based predictive EMS.

The main contributions of this paper are as follows: 1) Optimal control problem is reformulated in position domain, and then PMP approach is used to derive position-dependent boundary value problem (BVP), 2) Sensitivity differential equations are developed and solved which describe sensitivity of original BVP with respect to velocity uncertainty. Results show that sensitivity of position-dependent optimal state is negligible small compared to that of time-dependent optimal state.

The remainder of this paper is organized as follows: Section 2 includes an introduction to the FCHEV system configuration and system modelling for analytical approach. Section 3 briefly explains PMP theory, and then analytical optimal solution is derived in both time and position domain. In Section 4, first-order sensitivity analysis is introduced, and robustness of position-based predictive EMS is discussed. Finally, in Section 5, the summary and conclusions of this study are presented.

2 System-level FCHEV Model

This section deals with a system-level FCHEV model for optimal energy management strategy (EMS) [20]. FCHEV model consists of a fuel cell, battery, and vehicle. Fuel cell system acts as the main electrical energy source for system bus, and battery system must provide the electrical power for satisfying power required from driving cycle. This power bus relationship is expressed as follows:

$$P_{EM}(t) = P_{FC}(t) + P_{BT}(t) \quad (1)$$

where P_{EM} denotes electrical power required from electric motor, P_{FC} denotes required fuel cell power, and P_{BT} denotes required battery power.

In this study, system-level EMS is chosen, and simplified FCHEV model is used.

2.1 Fuel cell model

Hydrogen mass flow rate can be computed by using fuel cell current as shown below:

$$\dot{m}_{H_2} = \frac{N_{FC} M_{H_2}}{n_e F} \cdot I_{FC} \tag{2}$$

where N_{FC} denotes the number of cells in the fuel cell stack, M_{H2} denotes the molar mass of hydrogen, n_e denotes the number of electrons, and F denotes Faraday's constant.

With assumption of linear polarization curve and no auxiliary power, hydrogen mass flow rate can be described as function of required fuel cell power, and then it can be finally expressed as quadratic function of required fuel cell power by using Taylor's series approximation as shown below. (Appendix 1)

$$\dot{m}_{H_2} = \mu_1 \cdot P_{FC} + \mu_2 \cdot P_{FC}^2 \tag{3}$$

where $\mu_1 = \frac{N_{FC} M_{H_2}}{n_e F \cdot V_{FC.OC}}$, $\mu_2 = \frac{N_{FC} M_{H_2} R_{FC}}{n_e F \cdot V_{FC.OC}^3}$

2.2 Battery model

The battery model was developed based on the internal resistive equivalent circuit model, where a voltage source, resistor, and the load are connected in series. The battery current can be described as a function of required power, and then, approximated in the same way in the previous section. Finally, system dynamics of battery state of charge (SoC) as state variable is expressed by using the Coulomb counting method (Appendix 1), as follows:

$$\dot{x}(t) = f = \mu_3 \cdot P_{BT} + \mu_4 \cdot P_{BT}^2 \tag{4}$$

where $\mu_3 = -\frac{1}{Q_{\max} V_{BT.OC}}$, $\mu_4 = -\frac{R_{BT}}{Q_{\max} V_{BT.OC}^3}$

where $V_{BT.OC}$ denotes open circuit voltage, R_{BT} denotes internal resistance, and Q_{max} denotes the maximum battery capacity.

2.3 Vehicle model

The force demand profile of driving scenario can be determined using the longitudinal vehicle dynamic model, which is mainly dependent on the three force terms: rolling resistance, air drag resistance, and hill climbing resistance.

$$F_{demand} = m \cdot \dot{v} + c_1 \cdot v^2 + c_2 + c_3 \cdot \alpha \tag{5}$$

where $c_1 = \frac{1}{2} \rho_{air} \cdot A_f \cdot c_d$, $c_2 = c_r \cdot m \cdot g$, $c_3 = m \cdot g$

where v denotes vehicle velocity, ρ_{air} denotes ambient air density, A_f denotes front area, C_d denotes air drag coefficient, C_r denotes rolling resistance coefficient, m denotes vehicle mass, g denotes acceleration due to gravity, and angle α denotes road slope angle.

3 Optimal Control for FCHEVs

Optimal control of an FCHEV determines the optimal power split ratio between fuel cell system and battery system in order to minimize hydrogen consumption while guaranteeing the battery charge sustenance, wherein charge sustenance implies that the battery system must be maintain current SoC within admissible SoC range, and final SoC should be matched to initial SoC. In this section, PMP as horizon-optimization approach is introduced to derive analytical optimal solution in both time and position domain.

3.1 Optimal control problem

Optimal control uses dynamic models to minimize the cost function while satisfying constraint conditions. The optimal control problem is generally formulated in time domain, as follows:

$$\min\left(J = h\left(\mathbf{x}(t_f), t_f\right) + \int_{t_0}^{t_f} g\left(\mathbf{x}(t), \mathbf{u}(t), \boldsymbol{\omega}(t), t\right) dt \right) \tag{6}$$

$$\begin{aligned} \text{s.t. } & \dot{\mathbf{x}}(t) = \mathbf{f}\left(\mathbf{x}(t), \mathbf{u}(t), \boldsymbol{\omega}(t), t\right) \\ & \mathbf{x}(t_f) = \mathbf{x}_f \\ & \mathbf{x}(t) \in \mathbf{X}(t), \mathbf{u}(t) \in \mathbf{U}(t), \boldsymbol{\omega}(t) \in \mathbf{W}(t) \end{aligned}$$

where g denotes cost function, h denotes the terminal state cost that enforces final state to match the desired value. x, u, and ω represent the state variable, the control input, and disturbance, respectively.

3.2 PMP background

PMP is horizon optimization method that was developed based on the calculus of variations. PMP uses necessary conditions to derive boundary value problem (BVP), thus, it solves the optimal control problem analytically with lower computation burden and is often considered as a DP alternative.

3.2.1 State inequality constraints

The handling of state inequality constraints within PMP is in general nontrivial [21]. In this paper, a simple method is deployed to handle state inequality constraints within PMP. Concept of this method is that all state inequality constraints are converted into a single equality constraint by definition of a new state variable [22].

$$\dot{x}_n = f_n = \sum_{i=1}^{l}\left[\theta(-h_i)\cdot h_i^2(\mathbf{x}(t),t)\right]$$
$$\text{where } \theta(-h_i) = \begin{cases} 0, & \text{if } h_i \geq 0 \\ 1, & \text{else} \end{cases} \tag{7}$$

where h_i denotes i[th] state inequality constraints and l denotes the number of them. θ denotes the Heaviside step function. The fact that a new single equality constraint f_n is non-negative at all times implies state inequality constraints are all inactive.

3.2.2 Boundary value problem based on necessary conditions for optimality

Main idea of PMP is to minimize Hamiltonian function, thus, necessary conditions for optimality are used to derive boundary value problem [22]. In order to consider state inequality constraints, Hamiltonian function is newly augmented by a single equality constraint defined in previous section with using a new co-state p_n, as following equation.

$$H_n = H + p_n(t)\cdot f_n = g + \mathbf{p}^T(t)\cdot\mathbf{f} + p_n(t)\cdot f_n \tag{8}$$

where H denotes Hamiltonian function without consideration of state inequality constraints.
With using newly defined Hamiltonian function, the necessary conditions considering state constraints can now be derived for the case of fixed end time and state, as follows:

$$\dot{\mathbf{x}}(t) = \left(\frac{\partial H_n}{\partial \mathbf{p}}\right)^T = \mathbf{f},\ \dot{x}_n(t) = \frac{\partial H_n}{\partial p_n} = f_n \tag{9}$$

$$\dot{\mathbf{p}}(t) = -\left(\frac{\partial H_n}{\partial \mathbf{x}}\right)^T = -\left(\frac{\partial g}{\partial \mathbf{x}}\right)^T - \left(\frac{\partial \mathbf{f}}{\partial \mathbf{x}}\right)^T \mathbf{p}(t) - \left(\frac{\partial f_n}{\partial \mathbf{x}}\right)^T p_n(t) \tag{10}$$

$$\dot{p}_n(t) = -\frac{\partial H_n}{\partial x_n} = 0 \tag{11}$$

$$\mathbf{u}^*(t) = \arg\left\{\min_{\mathbf{u}(t)\in\mathbf{U}(t)} H_n(\mathbf{x}, x_n, \mathbf{u}, \mathbf{p}, p_n, t)\right\} \tag{12}$$

If control input inequality constraints do not explicitly depend on state variables, constrained optimal input can be easily derived as analytical solution. First, Hamiltonian function is augmented with using new Lagrange multiplier, as follows:

$$\begin{aligned} H_{nn} &= H_n + \boldsymbol{\lambda}^T(t)\cdot\mathbf{C} \\ &= g + \mathbf{p}^T(t)\cdot\mathbf{f} + p_n(t)\cdot f_n + \boldsymbol{\lambda}^T(t)\cdot\mathbf{C} \end{aligned} \tag{13}$$
$$\text{where } \lambda_i(t) = \begin{cases} \geq 0, & \text{if } C_i = 0 \text{ (active)} \\ = 0, & \text{if } C_i < 0 \text{ (inactive)} \end{cases}$$

where λ_i denotes Lagrange multipliers for constrained control input, and C_1 and C_2 imply (($-u) \leq 0$) and (($u-u_{max}) \leq 0$), respectively.
Then, necessary condition can be derived for computing constrained optimal input that generates minimum Hamiltonian function in the same way of unconstrained optimal control problem.

$$\frac{\partial H_{nn}}{\partial u} = 0 \tag{14}$$

Furthermore, boundary conditions are expressed as follows:

$$\begin{cases} \text{lost} & \text{if } t_f \text{ is fixed} \\ h_{t_f} + H_{nn}(t_f) = 0 & \text{if } t_f \text{ is free} \end{cases} \tag{15}$$

$$\begin{cases} x_i(t_f) = x_{i.f} & \text{if } x_i(t_f) \text{ is fixed} \\ p_i(t_f) = \dfrac{\partial h}{\partial x_i}(t_f) & \text{if } x_i(t_f) \text{ is free} \end{cases} \tag{16}$$

3.3 PMP realization of FCHEV

For PMP realization of FCHEV in time and position domain, all variables are first defined as follows: Cost (J) and state variable (x) is defined as hydrogen mass consumption and the battery SoC in both time and position domain, respectively. However, control input (u) are defined differently corresponding to domain type. In other words, in time domain, control input is defined as required fuel cell power, on the other hand, in position domain, it is defined as required fuel cell energy per distance.

3.3.1 In time domain

With given Eqs. ((3-4), (7)), equation (13) is used to express augmented Hamiltonian function of FCHEV problem in order to derive analytically constrained optimal control input as follows:

$$\begin{aligned} H_{nn}(t) &= \mu_1 u + \mu_2 u^2 \\ &+ p(t)\cdot\left(\mu_3(\omega-u) + \mu_4(\omega-u)^2\right) \\ &+ p_n(t)\cdot\left(\theta(-h_1)h_1^2 + \theta(-h_2)h_2^2\right) \\ &+ \lambda_1(t)\cdot(-u) + \lambda_1(t)\cdot(u-u_{\max}) \end{aligned} \tag{17}$$

$$\text{where } \omega = \begin{cases} \dfrac{F_{demand} \cdot v}{\eta} & \text{if } F_{demand} \geq 0 \\ \eta \cdot F_{demand} \cdot v & \text{else} \end{cases}$$

where ω denotes power demand, η denotes system efficiency including electric motor, inverter, transmission, and u_{max} denotes maximum required fuel cell power. h_l and h_2 imply (x_{max}-x) and (x-x_{min}), respectively.

Boundary value problem is derived by using PMP necessary conditions for optimality as follows:

$$\dot{x}(t) = \mu_3(\omega - u) + \mu_4(\omega - u)^2 \quad (18)$$

$$\dot{x}_n(t) = \theta(-h_1)h_1^2 + \theta(-h_2)h_2^2 \quad (19)$$

$$\dot{p}(t) = -2p_n\{-\theta(-h_1) \cdot h_1 + \theta(-h_2) \cdot h_2\} \quad (20)$$

$$\dot{p}_n(t) = 0 \quad (21)$$

The constrained optimal control input can be expressed as below. (Appendix 2)

$$u^*(t) = \begin{cases} 0 & \text{if } \omega \leq \omega_{\lim.1} \\ \dfrac{(-\mu_1 + 2\mu_4 p \cdot \omega + \mu_3 p)}{2(\mu_2 + \mu_4 p)} & \text{if } \omega_{\lim.1} < \omega < \omega_{\lim.2} \\ u_{\max} & \text{if } \omega \geq \omega_{\lim.2} \end{cases} \quad (22)$$

In FCHEV problem, both final time and final state are fixed, thus, boundary conditions can be simplified as follows:

$$x(t_0) = x(t_f) = x_0,\ x_n(t_0) = x_n(t_f) = 0 \quad (23)$$

3.3.2 In position domain

First, system models are transformed to be dependent on position, not time. Then, with position-dependent system models (Appendix 3), Hamiltonian function is expressed as function of position.

$$\begin{aligned} H_{d.nn}(s) &= \mu_1 u_d + \mu_2 u_d^2 v \\ &+ p_d(s) \cdot \left(\mu_3(\omega_d - u_d) + \mu_4(\omega_d - u_d)^2 v\right) \\ &+ \lambda_{d.1}(s) \cdot (-u_d) + \lambda_{d.2}(s) \cdot (u_d - u_{d.\max}) \end{aligned} \quad (24)$$

$$\text{where } \omega_d = \begin{cases} \dfrac{F_{demand}}{\eta} & \text{if } F_{demand} \geq 0 \\ \eta \cdot F_{demand} & \text{else} \end{cases}$$

where ω_d denotes required energy per distance, and $u_{d.max}$ denotes maximum required fuel cell energy per distance.

Position-dependent boundary value problem with constrained optimal control input is also derived in same way in previous section as follows:

$$\frac{dx_d(s)}{ds} = \mu_3(\omega_d - u_d) + \mu_4(\omega_d - u_d)^2 v \quad (25)$$

$$\frac{dx_{d.n}(s)}{ds} = \frac{1}{v}\left[\theta(-h_1)h_1^2 + \theta(-h_2)h_2^2\right] \quad (26)$$

$$\frac{dp_d(s)}{ds} = -\frac{2p_{d.n}}{v}\left[-\theta(-h_1) \cdot h_1 + \theta(-h_2) \cdot h_2\right] \quad (27)$$

$$\frac{dp_{d.n}(s)}{ds} = 0 \quad (28)$$

$$u_d^*(s) = \begin{cases} 0 & \text{if } \omega_d \leq \dfrac{\omega_{\lim.1}}{v} \\ \dfrac{(-\mu_1 + 2\mu_4 p_d \cdot \omega_d \cdot v + \mu_3 p_d)}{2(\mu_2 + \mu_4 p_d) \cdot v} & \text{if } \dfrac{\omega_{\lim.1}}{v} < \omega_d < \dfrac{\omega_{\lim.2}}{v} \\ u_{d.\max} & \text{if } \omega_d \geq \dfrac{\omega_{\lim.2}}{v} \end{cases} \quad (29)$$

Both final position and final state are fixed, thus, boundary conditions can be simplified as follows:

$$x_d(s_0) = x_d(s_f) = x_0,\ x_{d.n}(s_0) = x_{d.n}(s_f) = 0 \quad (30)$$

4 Sensitivity Analysis

This velocity uncertainty may significantly or hardly affect control performance corresponding to control schemes such as time-based or position-based predictive EMS. In this section, sensitivity analysis is performed through computation of sensitivity differentials of optimal solutions with respect to velocity uncertainty. First-order sensitivity coefficient provides direct information on the effect of a small variation in nominal velocity on time- and position-dependent optimal state.

4.1 Time-dependent sensitivity differential equations

If boundary value problem from PMP in time domain is solved by searching for initial co-states that satisfy all boundary conditions, its solution becomes optimal solution, which is considered as the nominal (unperturbed) optimal solution. This nominal optimal solution can be used to compute sensitivities of optimal states and co-states. First, sensitivities of optimal state and co-states with respect to velocity uncertainty are defined to formulate sensitivity dynamics as follows. Note that first-order sensitivity coefficient is applied to defined sensitivity variables.

$$\frac{\partial x^*}{\partial v} = z, \frac{\partial x_n^*}{\partial v} = z_n, \frac{\partial p^*}{\partial v} = \gamma, \frac{\partial p_n^*}{\partial v} = \gamma_n \quad (31)$$

Furthermore, because velocity uncertainty results in the increase/decrease in travel time, travel time sensitivity with respect to velocity uncertainty must be considered, and it is expressed as follows:

$$t = \int_{s_0}^{s} \frac{1}{v} ds \;\Rightarrow\; \frac{\partial t}{\partial v} = \int_{s_0}^{s} \left(-\frac{1}{v^2}\right) ds \quad (32)$$

Then, when all nonlinear equations ((18)-(21)) for boundary value problem are differentiated with respect to velocity uncertainty, following ordinary differential equation of sensitivity variables can be obtained as follows:

$$\frac{dz}{dt} = \frac{\partial f}{\partial \omega}\cdot\frac{\partial \omega}{\partial v} + \frac{\partial f}{\partial \omega}\cdot\frac{\partial \omega}{\partial t}\cdot\frac{\partial t}{\partial v} + \frac{\partial f}{\partial u^*}\cdot\frac{\partial u^*}{\partial v} \quad (33)$$

$$\frac{dz_n}{dt} = \frac{\partial f_n}{\partial x^*}\cdot z \quad (34)$$

$$\frac{d\gamma}{dt} = \frac{\partial \psi}{\partial p_n^*}\cdot\gamma_n + \frac{\partial \psi}{\partial x^*}\cdot z \quad (35)$$

$$\frac{d\gamma_n}{dt} = 0 \quad (36)$$

$$\frac{\partial u^*}{\partial v} = \frac{\partial \varphi}{\partial p^*}\cdot\gamma + \frac{\partial \varphi}{\partial \omega}\cdot\frac{\partial \omega}{\partial v} + \frac{\partial \varphi}{\partial \omega}\cdot\frac{\partial \omega}{\partial t}\cdot\frac{\partial t}{\partial v} \quad (37)$$

where derivation procedure of time-dependent sensitivity differential equation is addressed in Appendix 4.

Boundary conditions of time-dependent sensitivity variables can be expressed as follows.

$$z(t_0) = z(t_f) = z_n(t_0) = z_n(t_f) = 0 \quad (38)$$

4.2 Position-dependent sensitivity differential equations

In the same way in previous section, position-dependent sensitivities of optimal state and co-states with respect to velocity uncertainty are defined as follows.

$$\frac{\partial x_d^*(s)}{\partial v} = z_d, \frac{\partial x_{d.n}^*(s)}{\partial v} = z_{d.n}, \frac{\partial p_d^*}{\partial v} = \gamma_d, \frac{\partial p_{d.n}^*}{\partial v} = \gamma_{d.n} \quad (39)$$

Compared to travel time, travel position cannot be affected by velocity uncertainty, thus, consideration of travel position sensitivity is not needed.

Position-dependent sensitivity differential equations can be obtained in same way in previous section, it is expressed as below.

$$\frac{dz_d}{ds} = \frac{\partial f_d}{\partial v} + \frac{\partial f_d}{\partial \omega_d}\cdot\frac{\partial \omega_d}{\partial v} + \frac{\partial f_d}{\partial u_d^*}\cdot\frac{\partial u_d^*}{\partial v} \quad (40)$$

$$\frac{dz_{d.n}}{ds} = \frac{\partial f_{d.n}}{\partial v} + \frac{\partial f_{d.n}}{\partial x_d^*}\cdot z_d \quad (41)$$

$$\frac{d\gamma_d}{ds} = \frac{\partial \psi_d}{\partial v} + \frac{\partial \psi_d}{\partial p_{d.n}^*}\cdot\gamma_{d.n} + \frac{\partial \psi_d}{\partial x_d^*}\cdot z_d \quad (42)$$

$$\frac{d\gamma_{d.n}}{ds} = 0 \quad (43)$$

$$\frac{\partial u_d^*}{\partial v} = \frac{\partial \varphi_d}{\partial v} + \frac{\partial \varphi_d}{\partial p_d^*}\cdot\gamma_d + \frac{\partial \varphi_d}{\partial \omega_d}\cdot\frac{\partial \omega_d}{\partial v} \quad (44)$$

where derivation procedure of position-dependent sensitivity differential equation is addressed in Appendix 4.

Boundary conditions of position-dependent sensitivity variables can be expressed as follows.

$$z_d(s_0) = z_d(s_f) = z_{d.n}(s_0) = z_{d.n}(s_f) = 0 \quad (45)$$

4.3 Results

This section considers case study for comparative analysis on sensitivity of time- and position-dependent optimal state. Case study is performed to illustrate an important trend on state sensitivity and prove robustness of position-based predictive EMS for hilly road driving conditions. For simplicity, the predicted velocity profile is constant, and altitude profile is generated by using statistical hilly road generation method [14]. Thus, we can modify the simulation test cycle with the addition of the road grade profile to a velocity profile.

The maximum SoC bound is set to 80%, minimum SoC bound is set to 20%, and initial battery SoC is set to 50%. When SoC reaches the maximum SoC bound during braking, the supervisory controller switches from regenerative braking into conventional mechanical braking to prevent overcharging.

For comparative analysis, offline iterative search determines the initial values of co-states and that of co-state sensitivities for satisfying boundary conditions as well as necessary conditions.

4.3.1 Case study

Two goal of this subsections as follows: first one is to analyze the trend on magnitude of optimal state sensitivity with four different nominal value of constant velocity (70km/h, 90km/h, 110km/h, and

130km/h), and second one is to compare sensitivity of time- and position-dependent optimal state.

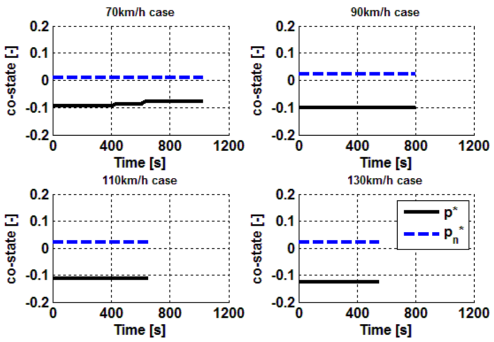

Figure 2: Co-states of PMP in time domain

The case of 70km/h represents the extreme driving condition that can activate state inequality constraints during driving. On the other hand, other cases represent normal driving conditions that cannot activate state inequality constraints. Co-state, p^*, of normal driving conditions have constant values and its value is changed with nominal value of velocity. Note that new co-costate, p_n^*, has same value for all normal driving conditions because it does not have effect on co-state dynamics, thus, it has meaningless value when state inequality constraints are inactive. In contrast, co-state of extreme driving condition has jump conditions that prevent violation of state inequality constraints in Figure 2. Furthermore, initial value of new co-state becomes important variable to determine the level of co-state jump under extreme driving condition such as 70km/h case.

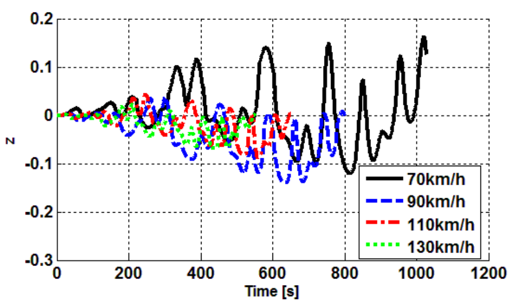

Figure 3: Sensitivity of time- and position-dependent optimal state for four driving conditions (70km/h, 90km/h, 110km/h, and 130km/h)

An important trend was observed from sensitivity trajectory of optimal state. Figure 3 shows how state sensitivity trajectories of different driving conditions are generated, and they change with the velocity nominal value. With increasing the velocity nominal value, state sensitivity trajectory is shifted to left due to the decrease in travel time at every position, moreover, RMS value and maximum absolute peak value of state sensitivity decrease as shown in Table 1.

Table 1: Quantitative comparison of sensitivity of time- and position-dependent optimal state for four driving conditions

	70 km/h	90 km/h	110 km/h	130 km/h
RMS value	0.062	0.063	0.034	0.029
Maximum peak value	0.162	0.140	0.089	0.068

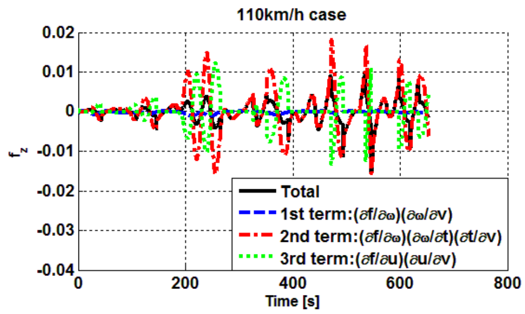

Figure 4: Analysis on state sensitivity dynamics in case of 110km/h as normal driving condition

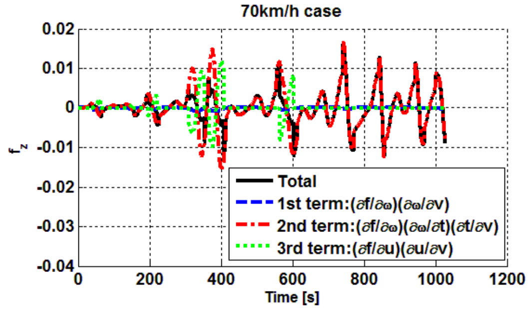

Figure 5: Analysis on state sensitivity dynamics in case of 70km/h as extreme driving condition

There are three terms which can have effect on state sensitivity dynamics as follows: first, second, and third term indicate variation resulting from the variation in power demand (ω), time (t), and optimal control input (u^*) by velocity uncertainty, respectively. For example, in case of 110km/h as normal driving condition, Figure 4 shows the general trend on the effect of each term on state sensitivity dynamics. It can be seen that first term is negligibly small, and second term is significant factor to affect state sensitivity dynamics, and third term that is generated when fuel cell system is operated tends to diminish the effect of second term.

As already mentioned before, both second and third term result in important trend on state sensitivity with different nominal velocity. Especially, magnitude of second term strongly depends on nominal velocity, thus, state sensitivity also becomes large with low nominal velocity despite of same position. Furthermore, as travel time approaches the final time, time sensitivity gradually increases (Equation (38)) and thus state sensitivity of each of all cases also increases (Figure 3).

In addition with the reason of the increased time sensitivity, another reason for the largest state sensitivity of extreme driving condition among all driving conditions is that third term that diminishes second term effect is rarely generated due to frequent operation of battery system, as shown in Figure 5. In case of extreme driving condition, jump conditions must be generated for achieving charge sustenance, thus, they result in frequent battery operation for using the stored braking energy.

However, sensitivity of position-dependent optimal state is significantly small for all driving conditions compared to that of time-dependent optimal state in Figure 6. Main reason of this is the robust property of position-dependent state trajectory; travel position cannot be affected by velocity uncertainty.

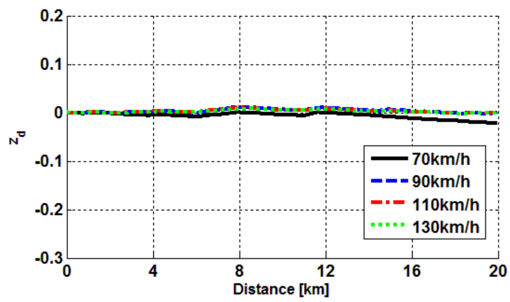

Figure 6: Sensitivity of position-dependent optimal state trajectory for four driving conditions (70km/h, 90km/h, 110km/h, and 130km/h)

4.3.2 Discussion

In terms of predictive EMS, one of the methods to use future information is use optimal SoC trajectory as a reference, explained in previous section. When velocity uncertainty exists, tracking nominal reference may result in large loss of optimality because it may lead to inefficient operation of fuel cell system by unnecessary battery charging/discharging. Figure 7 shows how much perturbed optimal SoC reference is deviated from nominal optimal SoC reference. It can be seen that time-dependent reference is easily distorted compared to position-dependent reference when plotted on a position vs. SoC plane. For this reason, position-dependent reference should be used for robustness of predictive EMS.

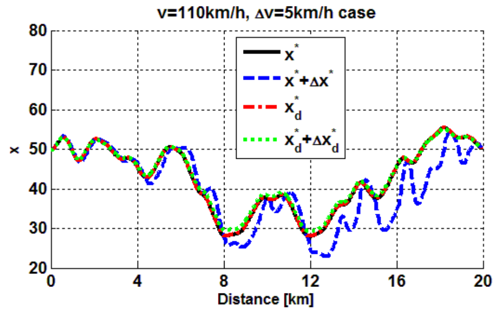

Figure 7: In case of 110km/h, optimal SoC trajectory computed from time-based and position-based PMP, and perturbed optimal SoC trajectory with velocity uncertainty (5km/h)

5 Conclusions

This paper studies robustness of position-based predictive EMS via sensitivity analysis with respect to velocity uncertainty. When velocity uncertainty presents, position-based predictive EMS as reference tracking controller has an advantage over time-based predictive EMS because position-dependent SoC reference is significantly less sensitive to velocity uncertainty compared to time-dependent SoC reference. PMP approach was selected to solve optimal control problem, and to calculate analytical sensitivity differentials for comparison analysis. Results showed that sensitivity of time-dependent optimal state decreases with the increase in nominal velocity, moreover, it increases as travel time approaches the final time. Therefore, in order to ensure robust and optimal performance with velocity uncertainty, position-based predictive EMS framework is recommended.

Appendix 1.

Polarization curve is assumed to be linear function as follows:

$$V_{FC} = V_{FC.OC} - R_{FC} I_{FC}$$

With using linear polarization curve, total derivation of hydrogen mass flow rate as quadratic function of required fuel cell power is as follows:

$$\dot{m}_{H_2} = \frac{N_{FC} M_{H_2}}{n_e F} \cdot I_{FC}$$

$$\approx \frac{N_{FC} M_{H_2}}{n_e F} \cdot \frac{V_{FC.OC} - \sqrt{V_{FC.OC}^2 - 4R_{FC} \cdot P_{FC}}}{2R_{FC}}$$
$$\approx \frac{N_{FC} M_{H_2}}{n_e F} \cdot \left\{ \frac{1}{V_{FC.OC}} \cdot P_{FC} + \frac{R_{FC}}{V_{FC.OC}^3} \cdot P_{FC}^2 \right\}$$
$$= \mu_1 \cdot P_{FC} + \mu_2 \cdot P_{FC}^2$$

Based on internal resistive equivalent circuit model, total derivation of battery SoC dynamics as quadratic function of required battery power is as follows:

$$\dot{x}(t) = -\frac{1}{Q_{\max}} I_{BT}(t)$$
$$= -\frac{1}{Q_{\max}} \cdot \frac{V_{BT.OC} - \sqrt{V_{BT.OC}^2 - 4R_{BT} \cdot P_{BT}}}{2 \cdot R_{BT}}$$
$$\approx -\frac{1}{Q_{\max} V_{BT.OC}} \cdot P_{BT} - \frac{R_{BT}}{Q_{\max} V_{BT.OC}^3} \cdot P_{BT}^2$$
$$= \mu_3 \cdot P_{BT} + \mu_4 \cdot P_{BT}^2$$

Appendix 2.

Constrained optimal control input can be analytically derived by using Eqs. ((14), (17)) in Section 3.2 and Section 3.3, as below.
If both input constraints are inactive,

$$\lambda_1(t) = 0,\ \lambda_2(t) = 0,\ \frac{\partial H_{nn}}{\partial u} = 0$$
$$\therefore u^*(t) = \frac{\left(-\mu_1 + 2\mu_4 p \cdot \omega + \mu_3 p\right)}{2\left(\mu_2 + \mu_4 p\right)}$$

If one of input constraints is active,

$$1)\ \lambda_1(t) \ge 0,\ \lambda_2(t) = 0,\ \frac{\partial H_{nn}}{\partial u} = 0$$
$$\therefore u^*(t) = 0 \quad \text{if } \omega \le \omega_{\lim.1}$$
$$\text{where } \omega_{\lim.1} = \frac{\mu_1 - \mu_3 p}{2\mu_4 p}$$
$$2)\ \lambda_2(t) \ge 0,\ \lambda_1(t) = 0,\ \frac{\partial H_{nn}}{\partial u} = 0$$
$$\therefore u^*(t) = u_{\max} \quad \text{if } \omega \ge \omega_{\lim.2}$$
$$\text{where } \omega_{\lim.2} = \frac{\mu_1 - \mu_3 p + 2\left(\mu_2 + \mu_4 p\right) u_{\max}}{2\mu_4 p}$$

Appendix 3.

The chain rule is used to transform system models to be dependent on position.

$$g_d(s) = \frac{dm_{H_2}}{ds} = \frac{dm_{H_2}}{dt}\frac{dt}{ds}$$
$$\approx \mu_1 \frac{dE_{FC}}{dt}\frac{dt}{ds} + \mu_2 \left(\frac{dE_{FC}}{dt}\frac{dt}{ds}\right)^2 \frac{ds}{dt}$$
$$= \mu_1 \frac{dE_{FC}}{ds} + \mu_2 \left(\frac{dE_{FC}}{ds}\right)^2 v(s)$$
$$f_{d.1}(s) = \frac{dx_d}{ds} = \frac{dt}{ds}\frac{dx_d}{dt}$$
$$\approx \mu_3 \frac{dE_{BT}}{ds} + \mu_4 \left(\frac{dE_{BT}}{ds}\right)^2 v(s)$$

where s denotes travel position, t denotes travel time.

Appendix 4.

Time-dependent sensitivity differential equations are derived as follows:

$$\frac{dz}{dt} = \frac{\partial}{\partial v} f\left(\omega(v,t), u^*\right)$$
$$= \frac{\partial f}{\partial \omega} \cdot \left(\frac{\partial \omega}{\partial v} + \frac{\partial \omega}{\partial t} \cdot \frac{\partial t}{\partial v}\right) + \frac{\partial f}{\partial u^*} \cdot \frac{\partial u^*}{\partial v}$$
$$\frac{dz_n}{dt} = \frac{\partial}{\partial v} f_n(x^*) = \frac{\partial f_n}{\partial x^*} \cdot \frac{\partial x^*}{\partial v} = \frac{\partial f_n}{\partial x^*} \cdot z$$
$$\frac{d\gamma}{dt} = \frac{\partial}{\partial v}\left(\frac{dp^*}{dt}\right) = \frac{\partial}{\partial v} \psi(p_n^*, x^*)$$
$$= \frac{\partial \psi}{\partial p_n^*} \cdot \frac{\partial p_n^*}{\partial v} + \frac{\partial \psi}{\partial x^*} \cdot \frac{\partial x^*}{\partial v} = \frac{\partial \psi}{\partial p_n^*} \cdot \gamma_n + \frac{\partial \psi}{\partial x^*} \cdot z$$
$$\frac{d\gamma_n}{dt} = 0$$
$$\frac{\partial u^*}{\partial v} = \frac{\partial}{\partial v} \varphi\left(p^*, \omega(v,t)\right)$$
$$= \frac{\partial \varphi}{\partial p^*} \cdot \frac{\partial p^*}{\partial v} + \frac{\partial \varphi}{\partial \omega} \cdot \left(\frac{\partial \omega}{\partial v} + \frac{\partial \omega}{\partial t} \cdot \frac{\partial t}{\partial v}\right)$$
$$= \frac{\partial \varphi}{\partial p^*} \cdot \gamma + \frac{\partial \varphi}{\partial \omega} \cdot \left(\frac{\partial \omega}{\partial v} + \frac{\partial \omega}{\partial t} \cdot \frac{\partial t}{\partial v}\right)$$
$$\text{where } \frac{\partial f}{\partial \omega} = \mu_3 + 2\mu_4\left(\omega - u^*\right)$$
$$\frac{\partial f}{\partial u^*} = -\left[\mu_3 + 2\mu_4\left(\omega - u^*\right)\right]$$
$$\frac{\partial f_n}{\partial x^*} = 2\left[-\theta(-h_1) \cdot h_1 + \theta(-h_2) \cdot h_2\right]$$
$$\frac{\partial \psi}{\partial p_n^*} = -2\left[-\theta(-h_1) \cdot h_1 + \theta(-h_2) \cdot h_2\right]$$
$$\frac{\partial \psi}{\partial x^*} = -2 p_n^* \left[\theta(-h_1) + \theta(-h_2)\right]$$
$$\frac{\partial \varphi}{\partial p^*} = \frac{\mu_1\mu_4 + \mu_2\mu_3 + 2\mu_2\mu_4\omega}{2\left(\mu_2 + \mu_4 p^*\right)^2}$$

$$\frac{\partial\varphi}{\partial\omega}=\frac{\mu_4 p^*}{\mu_2+\mu_4 p^*}$$

$$\frac{\partial\omega}{\partial v}=\begin{cases}\dfrac{3c_1\cdot v^2+c_2+c_3\cdot\alpha}{\eta} & \text{if } \omega\geq 0\\ \eta\left(3c_1\cdot v^2+c_2+c_3\cdot\alpha\right) & \text{else}\end{cases}$$

Position-dependent sensitivity differential equations are derived as follows:

$$\frac{dz_d}{ds}=\frac{\partial}{\partial v}f_d\left(v,\omega_d(v),u_d^*\right)$$
$$=\frac{\partial f_d}{\partial v}+\frac{\partial f_d}{\partial\omega_d}\cdot\frac{\partial\omega_d}{\partial v}+\frac{\partial f_d}{\partial u_d^*}\cdot\frac{\partial u_d^*}{\partial v}$$

$$\frac{dz_{d.n}}{ds}=\frac{\partial}{\partial v}f_{d.n}(v,x_d^*)=\frac{\partial f_{d.n}}{\partial v}+\frac{\partial f_{d.n}}{\partial x_d^*}\cdot\frac{\partial x_d^*}{\partial v}$$
$$=\frac{\partial f_{d.n}}{\partial v}+\frac{\partial f_{d.n}}{\partial x_d^*}\cdot z_d$$

$$\frac{d\gamma_d}{ds}=\frac{\partial}{\partial v}\left(\frac{dp_d^*}{ds}\right)=\frac{\partial}{\partial v}\psi_d(v,p_{d.n}^*,x_d^*)$$
$$=\frac{\partial\psi_d}{\partial v}+\frac{\partial\psi_d}{\partial p_{d.n}^*}\cdot\frac{\partial p_{d.n}^*}{\partial v}+\frac{\partial\psi_d}{\partial x_d^*}\cdot\frac{\partial x_d^*}{\partial v}$$
$$=\frac{\partial\psi_d}{\partial v}+\frac{\partial\psi_d}{\partial p_{d.n}^*}\cdot\gamma_{d.n}+\frac{\partial\psi_d}{\partial x_d^*}\cdot z_d$$

$$\frac{d\gamma_{d.n}}{ds}=0$$

$$\frac{\partial u_d^*}{\partial v}=\frac{\partial}{\partial v}\varphi_d\left(v,p_d^*,\omega_d(v)\right)$$
$$=\frac{\partial\varphi_d}{\partial v}+\frac{\partial\varphi_d}{\partial p_d^*}\cdot\frac{\partial p_d^*}{\partial v}+\frac{\partial\varphi_d}{\partial\omega_d}\cdot\frac{\partial\omega_d}{\partial v}$$
$$=\frac{\partial\varphi_d}{\partial v}+\frac{\partial\varphi_d}{\partial p_d^*}\cdot\gamma_d+\frac{\partial\varphi_d}{\partial\omega_d}\cdot\frac{\partial\omega_d}{\partial v}$$

where $\frac{\partial f_d}{\partial v}=\mu_4\left(\omega_d-u_d^*\right)^2$

$$\frac{\partial f_d}{\partial\omega_d}=\mu_3+2\mu_4\left(\omega_d-u_d^*\right)v$$

$$\frac{\partial f_d}{\partial u_d^*}=-\left[\mu_3+2\mu_4\left(\omega_d-u_d^*\right)v\right]$$

$$\frac{\partial f_{d.n}}{\partial v}=-\frac{1}{v^2}\left[\theta(-h_1)h_1^2+\theta(-h_2)h_2^2\right]$$

$$\frac{\partial f_{d.n}}{\partial x_d^*}=\frac{2}{v}\left[-\theta(-h_1)\cdot h_1+\theta(-h_2)\cdot h_2\right]$$

$$\frac{\partial\psi_d}{\partial v}=\frac{2p_{d.n}}{v^2}\left[-\theta(-h_1)\cdot h_1+\theta(-h_2)\cdot h_2\right]$$

$$\frac{\partial\psi_d}{\partial p_{d.n}^*}=-\frac{2}{v}\left[-\theta(-h_1)\cdot h_1+\theta(-h_2)\cdot h_2\right]$$

$$\frac{\partial\psi_d}{\partial x_d^*}=-\frac{2p_{d.n}}{v}\left[\theta(-h_1)+\theta(-h_2)\right]$$

$$\frac{\partial\varphi_d}{\partial v}=\frac{\mu_1-\mu_3 p_d^*}{2\left(\mu_2+\mu_4 p_d^*\right)\cdot v^2}$$

$$\frac{\partial\varphi_d}{\partial p_d^*}=\frac{\mu_1\mu_4+\mu_2\mu_3+2\mu_2\mu_4\omega_d v}{2\left(\mu_2+\mu_4 p_d^*\right)^2 v}$$

$$\frac{\partial\varphi_d}{\partial\omega_d}=\frac{\mu_4 p_d^*}{\mu_2+\mu_4 p_d^*}$$

$$\frac{\partial\omega_d}{\partial v}=\begin{cases}\dfrac{2c_1\cdot v}{\eta} & \text{if } \omega_d\geq 0\\ \eta\cdot\left(2c_1\cdot v\right) & \text{else}\end{cases}$$

Acknowledgments

This work was supported by the National Research Foundation of Korea (NRF) grant funded by the Korea Government (MSIP) (No.2010-0028680).

References

[1] A. A. Malikopoulos, *Supervisory Power Management Control Algorithms for Hybrid Electric Vehicles: A Survey*, IEEE Transactions on Intelligent Transportation Systems, 15(2014), 1869-1885.

[2] D. Feroldi, M. Serra, and J. Riera, *Energy Management Strategies based on efficiency map for Fuel Cell Hybrid Vehicles*, Journal of Power Sources, 190(2009), 387-401.

[3] T. Hofman, M. Steinbuch, R. Van Druten, and A. Serrarens, *Rule-based energy management strategies for hybrid vehicles*, International Journal of Electric and Hybrid Vehicles, 1(2007), 71-94.

[4] J. Wu, C. H. Zhang, and N. X. Cui, *Fuzzy energy management strategy for a hybrid electric vehicle based on driving cycle recognition*, International Journal of Automotive Technology, 13(2012), 1159-1167.

[5] R. E. Bellman, *Dynamic programming*, Princeton University Press, 1957.

[6] A. Brahma, Y. Guezennec, and G. Rizzoni, *Optimal energy management in series hybrid electric vehicles*, in Proceedings of the American Control Conference, (2000), 60-64.

[7] C. C. Lin, H. Peng, J. W. Grizzle, and J. M. Kang, *Power management strategy for a parallel hybrid electric truck*, IEEE Transactions on Control Systems Technology, 11(2003), 839-849.

[8] N. Kim, S. Cha, and H. Peng, *Optimal control of hybrid electric vehicles based on Pontryagin's minimum principle*, IEEE Transactions on Control Systems Technology, 19(2011), 1279-1287.

[9] C. H. Zheng, G. Q. Xu, Y. I. Park, W. S. Lim, and S. W. Cha, *Comparison of PMP and DP in fuel*

cell hybrid vehicles, International Journal of Automotive Technology, 15(2014), 117-123.

[10] G. Paganelli, G. Ercole, A. Brahma, Y. Guezennec, and G. Rizzoni, *General supervisory control policy for the energy optimization of charge-sustaining hybrid electric vehicles*, JSAE Review, 22(2001), 511-518.

[11] P. Rodatz, G. Paganelli, A. Sciarretta, and L. Guzzella, *Optimal power management of an experimental fuel cell/supercapacitor- powered hybrid vehicle*, Control Engineering Practice, 13(2005), 41-53.

[12] J. Park and J. H. Park, *Development of equivalent fuel consumption minimization strategy for hybrid electric vehicles*, International Journal of Automotive Technology, 13(2012), 835-843.

[13] J. Han, Y. Park, and D. Kum, *Optimal adaptation of equivalent factor of equivalent consumption minimization strategy for fuel cell hybrid electric vehicles under active state inequality constraints*, Journal of Power Sources, 267(2014), 491-502.

[14] J. Han, D. Kum, and Y. Park, *Impact of hilly road information on fuel economy of FCHEV based on parameterization of hilly roads*, International Journal of Automotive Technology, 15(2014), 283-290.

[15] D. Lee, S. W. Cha, A. Rousseau, N. Kim, and D. Karbowski, *Optimal Control Strategy for PHEVs using Prediction of Future Driving Schedule*, in Proceedings of 26th Electric Vehicle Symposium 2012, (2012), 2339-2348.

[16] F. Tianheng, Y. Lin, G. Qing, H. Yanqing, Y. Ting, and Y. Bin, *A supervisory control strategy for plug-in hybrid electric vehicles based on energy demand prediction and route preview*, IEEE Transactions on Vehicular Technology, 99(2014), 1-10.

[17] F. Lacandia, L. Tribioli, S. Onori, and G. Rizzoni, *Adaptive energy management strategy calibration in PHEVs based on a sensitivity study*, SAE International Journal of Alternative Powertrains, 2(2013), 443-455.

[18] D. Ambuhl and L. Guzzella, *Predictive reference signal generator for hybrid electric vehicles*, IEEE Transactions on Vehicular Technology, 58(2009), 4730-4740.

[19] T. van Keulen, B. de Jager, A. Serrarens, and M. Steinbuch, *Optimal energy management in hybrid electric trucks using route information*, Oil and Gas Science and Technology, 65(2010), 103-113.

[20] L. Guzzella and A. Sciarretta, *Vehicle propulsion systems: introduction to modelling and optimization*, Springer, 2005

[21] R. F. Hartl, S. P. Sethi, and R. G. Vickson, *A Survey of the Maximum Principles for Optimal Control Problems with State Constraints*, SIAM Review, 37(1995), 181-218.

[22] D. E. Kirk, *Optimal control theory: an introduction*, Prentice-Hall, 1970

Authors

Jihun Han received his B.S. and M.S. degrees in Mechanical Engineering from Korea Advanced Institute of Science and Technology (KAIST), South Korea, in 2009 and 2011, respectively. He is currently Ph.D candidate at Mechanical engineering at KAIST. His research interests include optimal control and vehicle dynamics and control.

Dongsuk Kum received his Ph.D. degree in mechanical engineering from the University of Michigan, Ann Arbor, in 2010. From 2010 to 2012, he worked at the General Motors R&D Propulsion Systems Research Laboratory in Warren, MI as a visiting research scientist. Since 2012, he has been a faculty member at the Korea Advanced Institute of Science and Technology (KAIST) in Daejeon, Korea. His research interests include modeling, optimal control, and feedback control with an emphasis on their applications to hybrid electric vehicles and autonomous driving systems.

Youngjin Park received his B.S. and M.S. degrees in Mechanical Engineering from Seoul National University, South Korea, in 1980 and 1982, respectively. He then received his Ph.D. degree in Mechanical Engineering from University of Michigan, USA, in 1987. From 1987 to 1988, he worked as a research fellow at University of Michigan. He also worked as an assistant professor at NJIT, NJ, from 1988 to 1990. He joined the faculty of KAIST in 1990, where he is a Professor of Mechanical Engineering. His research interests include general control theories, virtual audio synthesis, active control of noise and vibration, system identification